D. Chellaganesh, M. Adam Khan*, J. T. Winowlin Jappes and S. Sathiyanarayanan

Cyclic Oxidation and Hot Corrosion Behavior of Nickel–Iron-Based Superalloy

DOI 10.1515/htmp-2016-0130
Received June 27, 2016; accepted January 9, 2017

Abstract: The high temperature oxidation and hot corrosion behavior of nickel–iron-based superalloy are studied at 900 ° and 1000 °C. The significant role of alloying elements with respect to the exposed medium is studied in detail. The mass change per unit area was catastrophic for the samples exposed at 1000 °C and gradual increase in mass change was observed at 900 °C for both the environments. The exposed samples were further investigated with SEM, EDS and XRD analysis to study the metallurgical characteristics. The surface morphology has expressed the in situ nature of the alloy and its affinity toward the environment. The EDS and XRD analysis has evidently proved the presence of protective oxides formation on prolonged exposure at elevated temperature. The predominant oxide formed during the exposure at high temperature has a major contribution toward the protection of the samples. The nickel–iron-based superalloy is less prone to oxidation and hot corrosion when compared to the existing alloy in gas turbine engine simulating marine environment.

Keywords: superalloy, oxidation, corrosion, salt, oxides

Introduction

The hot section of gas turbine engine component will access large amount of hot air and fuels with atmospheric contaminants during combustion/propulsion. The corrosion issues are similar for all the applications [1]. In general the turbine component operates between the temperatures of 640°C and 1350 °C. The composition of hot gas/flue gas which enters the turbine is the key factor for material degradation of the turbine component. The oxidation cannot be avoided partially or completely by altering the environment or materials quality [2]. The air to fuel ratio is approximately 0.12–0.18 M of oxygen during combustion that leads to highly oxidizing environment to the metals. The sulfur from the fuel and sodium chlorides from the ingested air (marine environment) will react to form sodium sulfates as molten salt. The deposits of molten salt on the hot section will result in accelerated oxidation or sulfidation attack on the metals [3]. Sulfidation is a form of corrosion in which sulfur penetrates into the metal locally to precipitate chromium [4]. Various mechanisms have been involved while accelerated corrosion attack; the salt fluxing model is probably the most widely accepted. The metal oxides may dissolve in Na_2SO_4 as anionic species (basic fluxing) or cationic species (acid fluxing), depending on the salt composition. During combustion of oil/fuel in gas turbine engine, the low melting (at 600 °C) contaminants are formed in the combination of vanadium, sodium and sulfur. Salt is acidic when it is high in SO_3 and basic when low in SO_3. The detailed information on the hot corrosion mechanism by salt fluxing can also be found in gas turbine books [5].

The turbines hot gas path is made up of special alloys to withstand high temperature application. The oxidations of alloys are more problematic than the pure metals. The nickel based alloys are extensively used in gas turbine applications due to its high working temperature and aggressive environment [6]. But it undergoes atmospheric deterioration of material resulting from erosion and corrosion, especially to meet the needs of the hot gas path components [7]. Many researchers have discussed the basic physical metallurgy of the alloy and its research on corrosion [8, 9]. When Ni–Cr–Al-based alloys are exposed to high temperature applications all possible oxides are formed during incubation and thermodynamically oxides protect the surface of the components. At the lower temperatures, it has a basic character due to the release of oxygen ions when sulfur is absorbed by the metal. In either condition, it can attack the amphoteric oxides, Cr_2O_3 and Al_2O_3 but Al_2O_3 is more resistant to acid

***Corresponding author: M. Adam Khan,** Department of Mechanical Engineering, International Research Centre (IRC), Kalasalingam University, Krishnankoil, Tamil Nadu, India,
E-mail: adamkhanm@gmail.com
D. Chellaganesh, Department of Mechanical Engineering, Kalasalingam University, Krishnankoil, Tamil Nadu, India,
E-mail: mechchellam@gmail.com
J. T. Winowlin Jappes, Research Faculty, Mechanical Engineering, International Research Centre (IRC), Kalasalingam University, Krishnankoil, Tamil Nadu, India
S. Sathiyanarayanan, Corrosion and Materials Protection Division, CSIR-Central Electrochemical Research Institute, Karaikudi 630 003, Tamilnadu, India

fluxing and Cr_2O_3 is more resistant to basic fluxing. The deep oxidation and corrosion behavior of the superalloys are explained by many researchers for certain applications. This study differs from existing research with respect to the material and simulating environment.

In this paper, the cyclic oxidation and hot corrosion behavior studies on Hastelloy X were carried out at two different temperatures (900 °C and 1000 °C). The samples were exposed directly to (i) air and (ii) the combination of molten salt 75 % Na_2SO_4–25 % NaCl (in wt. %). The exposed samples were further studied with metallurgical characterization techniques for better illustration and discussion of the results.

Materials and methods

The Hastelloy X is the candidate material for oxidation and hot corrosion studies. The alloy X is widely used in jet engine tailpipes, afterburner components, cabin heaters, nuclear reactors and other aircraft parts [10–14]. The nominal composition of the material is as follows: Ni – 47 %, Cr – 22 %, Mo – 9 %, W – 0.60 %, Fe – 18.50 %, Si – 1 %, C – 0.1 % and traces of Mn, Al, Ti, Cu, P, B & S. The samples are sliced to a dimension of 10 × 10 × 3 mm using wire electrical discharge machining. Subsequently, the samples were cleaned and polished through conventional metallographic methods. The samples after metallographic preparation were exposed to elevated temperatures at 900 ° and 1000 °C with and without salt environment. The salt environment was simulated in the combination of Na_2SO_4 and NaCl [75 % Na_2SO_4 + 25 % NaCl (in wt. %)] for hot corrosion studies. The concentration of 3–5 mg/cm^2 of salt as a paste was applied on the surface area of the samples [15–18]. Then the samples were kept on the ceramic boats to preheat (upto 250 °C) and to eliminate the moisture content in the salt for an hour in a furnace. Cyclic oxidation studies were carried out in air after sample preparation. The samples are exposed at 900 ° and 1000 °C for 10 cycles repeatedly for 5 hours (as soaking time) each completing 50 h. After every cycle, the samples were air cooled and weighed for mass change. The same procedure was repeated for all samples.

The high-resolution scanning electron microscope (Make: Zeiss) fitted with Energy Dispersive Spectroscopy (Make: Brukers, GmbH) for compositional analysis. Further, the presence of predominant oxides is confirmed through the X-ray diffraction with CuKα radiation (λ = 1.541 nm) (Make: Brukers).

Results and discussion

Oxidation and hot corrosion

The oxidation and hot corrosion behavior of the Hastelloy X were studied at 900 ° and 1000 ° C. Figure 1 shows the photo image of the samples exposed at 1000 °C to molten salt and atmospheric air for hot corrosion and oxidation studies. It is clear to note that the surface of the sample exposed to molten salt has been prone to trivial deterioration under molten salt; however in air, the sample has good resistance to oxidation.

At each and every cycle the changes in mass changes were recorded and plotted for each samples in the graph (Figure 2). The samples have undergone minor changes in mass change per unit area (≤ 1 mg/cm^2) for fifty hours during the hot corrosion and oxidation studies at 900 °C.

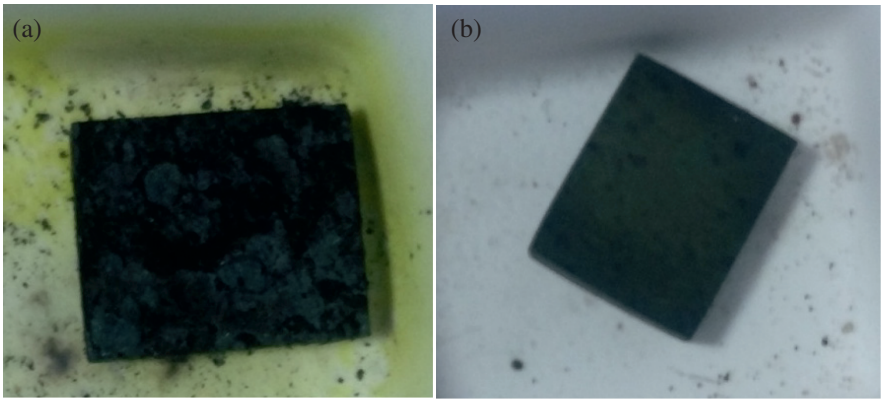

Figure 1: The photo image of the samples exposed to 1000 °C to (a) Na_2SO_4 and NaCl [75 % Na_2SO_4 + 25 % NaCl (in wt. %)] and (b) atmospheric air.

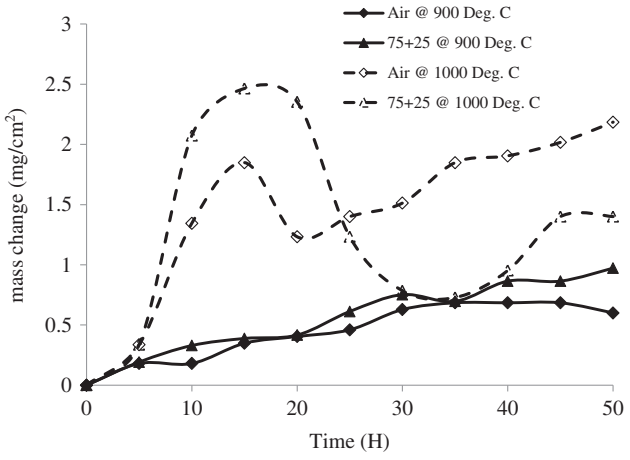

Figure 2: Mass change per unit area with respect to exposed temperature and environment.

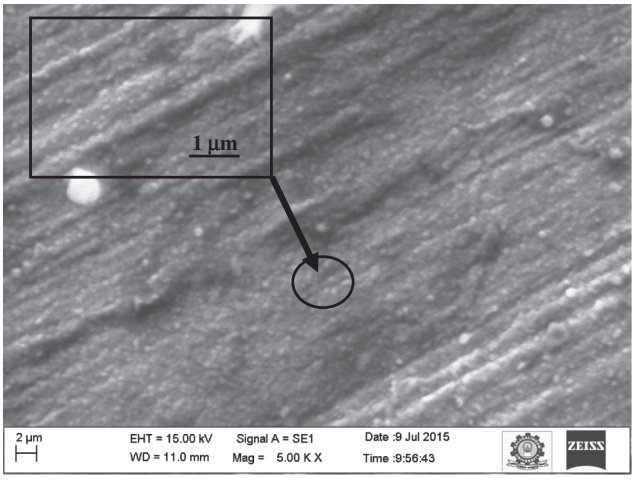

Figure 3: SEM micrograph of Hastealloy X exposed to air at 900 °C (Insert: nucleation of oxides observed under higher magnifications).

In the early literature, the researchers have reported that, at 900 °C the change in mass is gradual and the changes are gradual without any fluctuation for all the nickel-based superalloys [15, 19]. On other hand, the behavior of the same samples at 1000 °C has wide variations in mass changes at the beginning and matured over the subsequent cycles. The average mass change per unit area is 2 mg/cm^2. The change in variation might be due to the high impact of electrochemical kinetic reactions of Cr and Fe at elevated temperatures. During the inception, the transportation of iron and chromium ions prevailed over the surface of the samples through oxide scale formation. The occurrence of change in mass was observed at the beginning and dwells at 20 h. With reference to Figure 1(a), the fissure on the surface of the exposed sample at 1000 °C might be the evidence for change in mass. The experimental results are studied in detail through SEM, EDS and XRD analysis in the following sections.

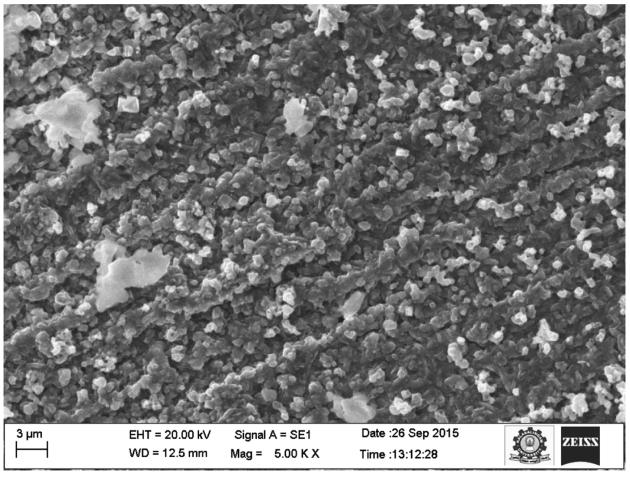

Figure 4: SEM micrograph showing oxidize nucleation on Hastealloy X exposed to air at 1000 °C.

SEM and EDS analysis

Figures 3 and 4 show the SEM micrograph of the alloy exposed at 900 ° and 1000 °C for oxidation studies. The exposed surface has deteriorated slightly which can be observed only under higher magnification of microscope. Enze [20] reported the same morphology for the DZ68 superalloy exposed at 900 °C. However, in other nickel-based superalloys the surface morphology was observed in the form of agglomerates and precipitates on the surface of the samples exposed at same temperature [21, 22]. The oxide formation depends on various factors and the reaction mechanism is quite different. The oxidation starts with adsorption of the oxygen molecules from the atmosphere and then followed the nucleation of oxides over the surface of the samples (Figure 5). This reaction occurs naturally on prolonged exposure of the samples at elevated temperatures. Severe oxidation will also lead to scale formation and spalling of the oxides on prolonged exposure. Even after fifty hours of exposure there is no such vulnerable kinetic reactions existed on the surface of the sample Hastelloy as reported by other researchers on nickel-based superalloy.

The SEM–EDS analysis report along with the image mapping of the samples that were exposed at 900 ° and 1000 °C are shown in Figures 6 and 7. As indicated in the SEM micrographs the oxide scale formation

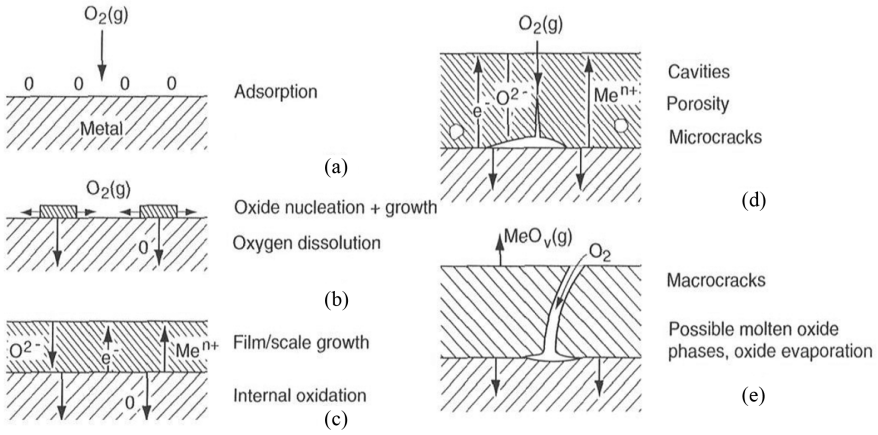

Figure 5: Sequence of oxide scale formation of a metal during high temperature oxidation.

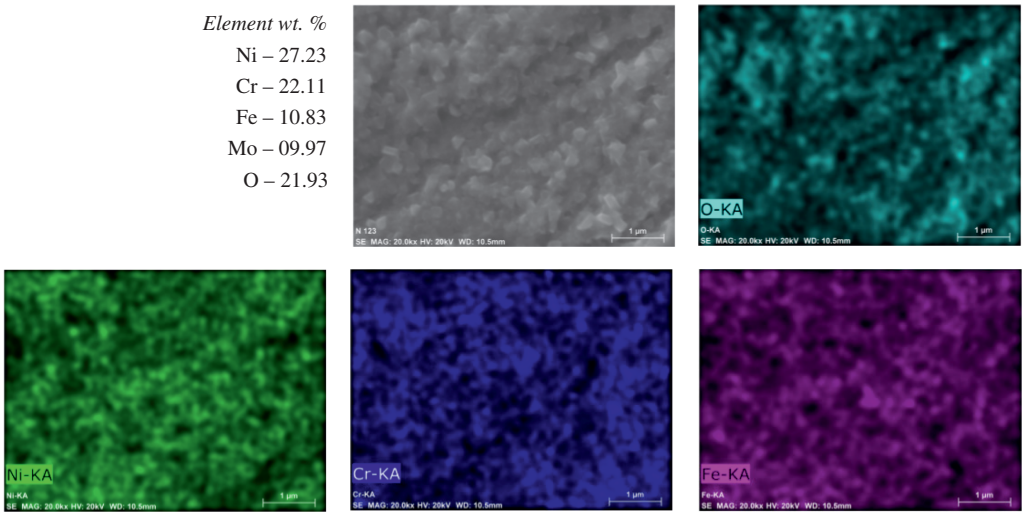

Figure 6: The SEM, EDS and image mapping of the sample exposed to air at 900 °C.

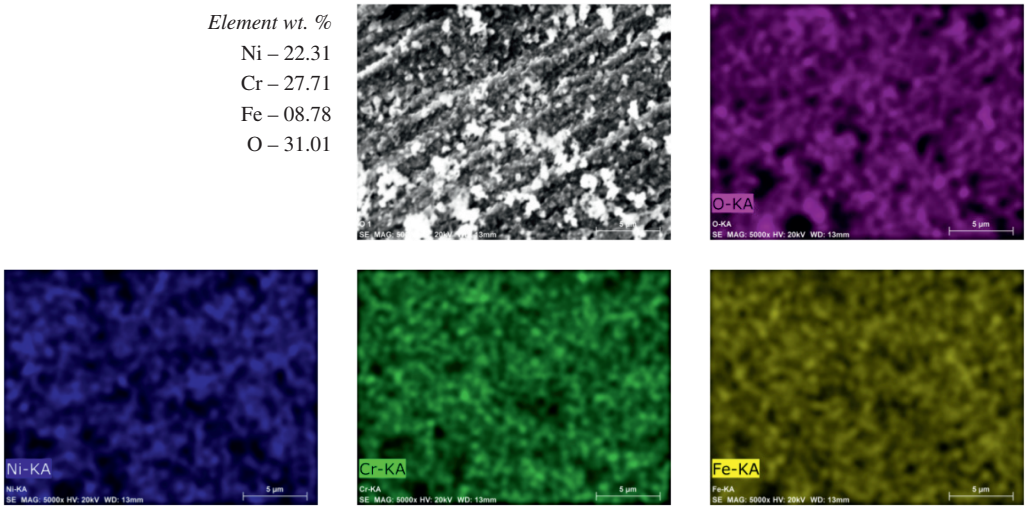

Figure 7: SEM, EDS and image mapping of the alloy X exposed to air at 1000 °C.

is slow and distribution of the oxides is uniform. Image mapping reproduces the elements/oxide formed over the exposed surface of the samples at 900 ° and 1000 °C. The image mapping indicates the distribution of major alloying elements Ni, Cr and Fe after oxidation. It also shows that oxygen the main element distributed over the exposed surface. At 1000 °C the surface of the alloy has undergone uniform oxidation and oxides are in the form of agglomerates/precipitates compared to the sample at 900 °C. The oxide elements weight percentage varied with respect to the exposed temperature. In both the situation the oxygen distribution is strong than alloying elements. The formation of chromium oxide is relatively fast than the nickel and iron oxides at elevated temperatures. On prolonged exposure the protective Cr_2O_3 (Chromia) will react with other metal oxides (metal 'M' may be Ni, Fe or Co) to form spinel (for example Nichromite–$NiCr_2O_4$) and partial dissolution occurs with molten salt at elevated temperature [18–21]. The Brukers–EDS spectra analysis report has revealed that Cr oxide is the most dominating (Cr_2O_3 – 40 %) oxide compared to the oxides of nickel and iron (NiO – 28 % and FeO – 11.3 %) for the sample exposed at 1000 °C and mere changes for the sample at 900 °C.

Figure 8 shows the surface morphology of the sample with Na_2SO_4–NaCl (75 + 25 wt. %) salts exposed at 1000 °C for fifty hours. The oxides are not uniformly distributed on the surface and it is in the form of whiskers nucleating in the structure of broccoli. On prolonged exposure continuous micro pores has lead to micro crack and spalling of oxides scales. Many researchers have reported that the surface oxides of the superalloys at elevated temperatures on prolonged exposure will be observed in the form of precipitates and agglomerates [23, 24]. However, for Hastelloy under higher magnification, the structure of oxide reveals like an outcropping of metal as a flakes in a shape of polycrystalline (Figure 9). This has not been observed in any report of early research of any superalloys or metals exposed at elevated temperatures with a molten salt for hot corrosion studies. The pegging of oxides in the

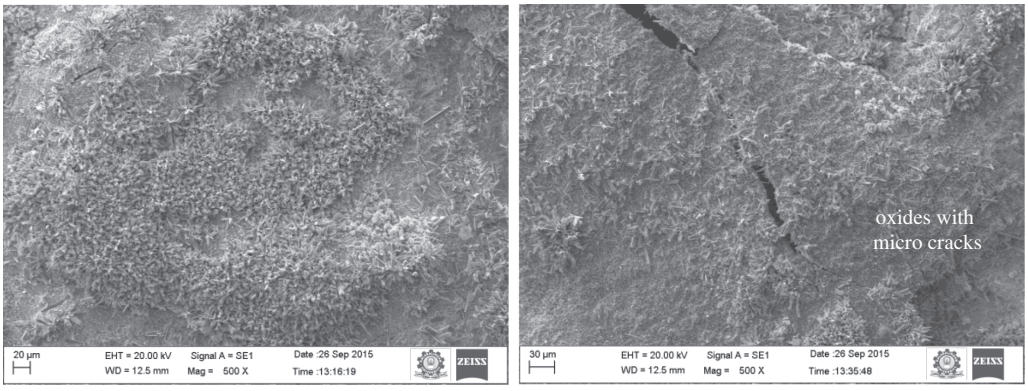

Figure 8: SEM micrograph indicating the oxides in the form of whiskers and micro cracks on the surface of the exposed samples.

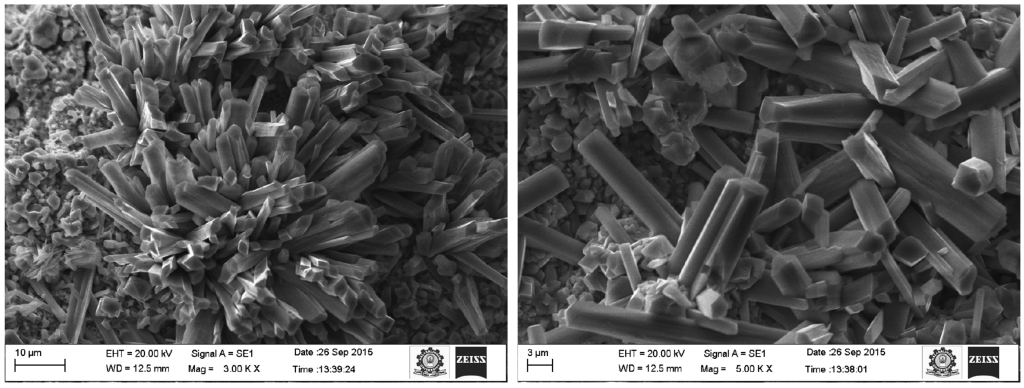

Figure 9: Structure of oxides observed under high magnification of the sample exposed with molten salt at 1000 °C.

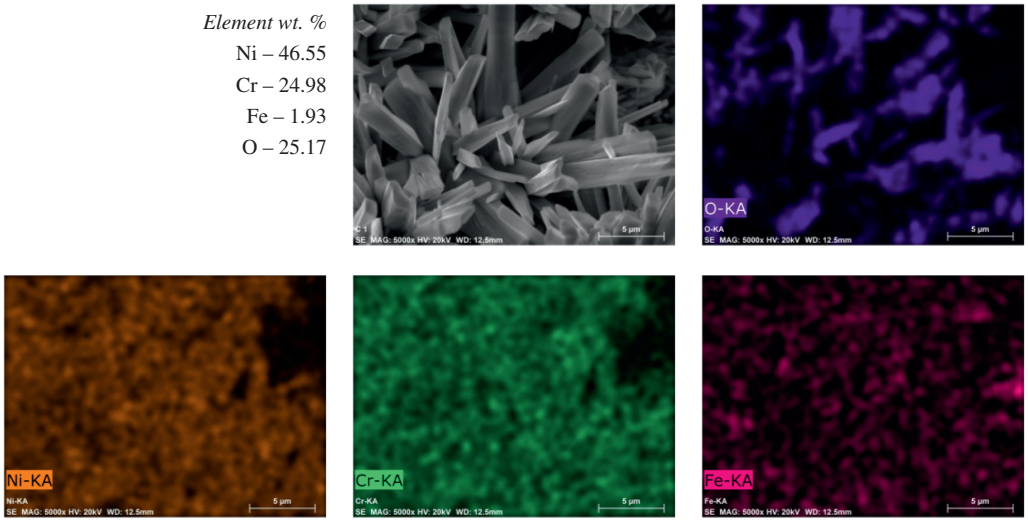

Figure 10: SEM, EDS and Image mapping of the alloy X exposed at 1000 °C with Na_2SO_4–NaCl (75 + 25 wt. %) salts.

form of flakes may be due to the reaction of alloying elements with the molten salt. Figure 10 shows the SEM, EDS and image mapping of the hot corrosion sample. Based on alloy sulfidation, the Ellingham-type phase stability diagram indicates that the role of M – O – Na – S (where, 'M' can be Ni, Co, Fe, Cr and A) reacts through grain boundaries and form metal oxides and metal sulfides [25]. In present study the predominant oxide formations are Cr_2O_3 – 40.50 %, NiO – 28.39 % and FeO – 11.30 % along with minor traces. With reference to the oxide solubilities [22], the NiO and FeO are basic oxides and Cr_2O_3 the acid oxide which was found balanced. Thus the surface of the metal oxides prone to protect the alloy from further degradation and the same has been evidently proved from the graph Figure 2. To study in detail, the oxides are removed/cleaned from the surface of the sample with acetone and further subjected to superficial analysis. Figure 11 expresses the presence of micro pores and voids over the adjunct layer of the exposed alloy. It proves that the metal oxides in the form of polycrystalline have been drawn out due to the chemical affinity. The behavior of the alloy was found uniform and chronic. Further the samples were subjected to elemental analysis with the help of EDS and reported in Figure 12. The variation in oxide formation is noticed as Cr_2O_3 – 35.35 %, NiO – 26.83 % and FeO – 34.70 %. It is clear to infer that the Cr (wt.%) is less in fall and this is due to acidic fluxing cum dissolution of protective oxides. Graham [26] and Guo [27] reported a similar observations for superalloys exposed to mixed salt environment at elevated temperatures and vaporization kinetics for Cr_2O_3.

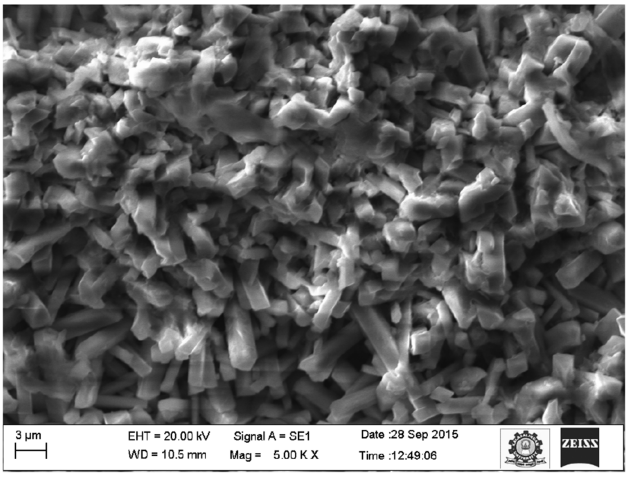

Figure 11: Surface morphology of the exposed sample after removal of oxides.

XRD analysis

Figure 13 shows the formation of predominant oxides during the oxidation and hot corrosion behavior of Hastelloy exposure at 900 °C and 1000 °C. The XRD results are similar to Hastelloy exposed to both the temperatures at different environments. The predominant oxides such as NiO, Cr_2O_3 and Fe_2O_3 from the EDS analysis are evidently proved through XRD peak. It is also confirmed that the chromium oxides have been reacted with the iron and nickel to form spinels in the form of Nichromite and Chromite. The XRD analysis reports spinel oxide score 14 (Ref: 98-001-7318 for

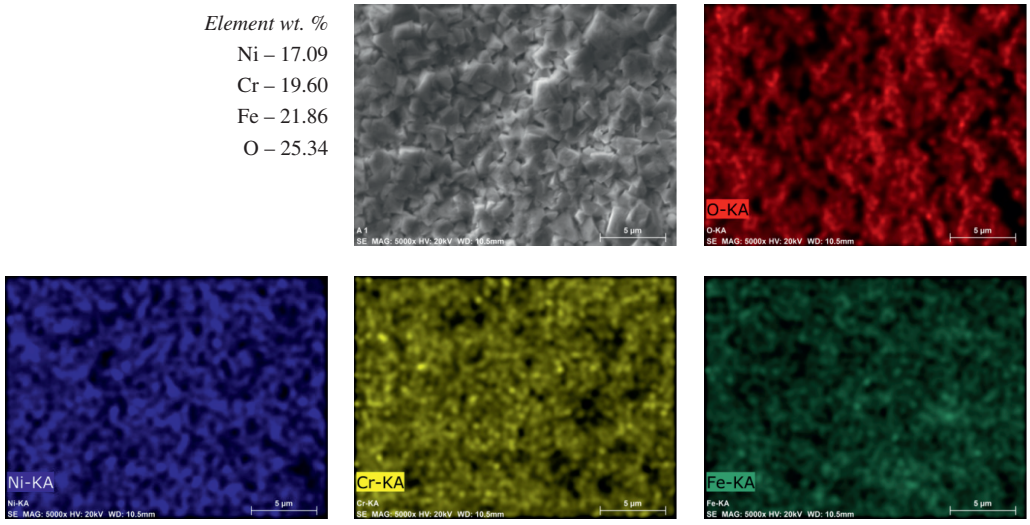

Figure 12: SEM, EDS and image mapping of the exposed sample after removal of oxides.

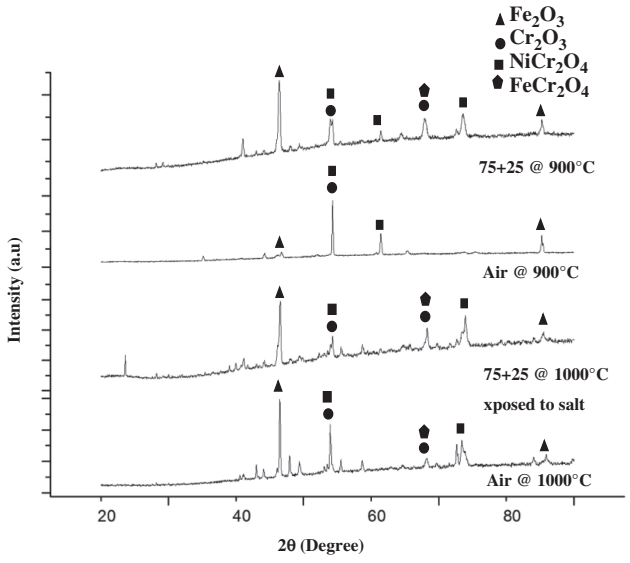

Figure 13: XRD peaks show the predominant oxides formed during oxidation and hot corrosion studies on Hastelloy X.

Nichromite Cr_2 Ni_1 O_4) and 6 (Ref: 98-005-0990 for Chromite Cr_2 Fe_1 O_4) respectively. The addition of iron to high nickel and chromium alloy will result in precipitate oxides in the form of crystal while exposed above 850 °C for 2 days and the $FeCr_2O_4$ will nucleate from the grain boundary oxide region where alloy will disappear [28–30]. Thus the alloy grain changes to grain oxides as shown in Figures 10 and 12. The presences of dense spinel may be protecting the surface from severe corrosion/oxidation at elevated temperatures.

Conclusions

The high temperature oxidation and hot corrosion studies were carried out at 900 ° and 1000 °C for fifty hours. The high temperature oxidation studies were performed in atmospheric air (without salt environment) and hot corrosion with a molten salt (Na_2SO_4 + NaCl) environment.

1. There is no significant variation in oxidation and hot corrosion at 900 °C. However, at 1000 °C the sample shows catastrophic behavior of the alloy due to its affinity toward the molten salt.
2. During oxidation, the nucleations of oxides are uniform along the grain boundaries in size less than a micron.
3. The oxides in the form of polycrystalline shape are observed on prolonged exposure of the samples with molten salt exposed at elevated temperatures. The oxides are in the form of precipitates due to the electrochemical behavior of iron and sulfur at elevated temperatures.
4. The XRD analysis also proved the presence of spinels in the form of Nichromite and Chromite along with the major oxides. The presence of dense spinels will be the barrier to protect the adjunct layer of the alloy from oxidation and corrosion.

References:

[1] E. Kosieniak, K. Biesiada, J. Kaczorowski and M. Innocenti, J. Fail. Anal. Prev., 12(3) (2012) 330–337.
[2] G.Y. Lai, High Temperature Corrosion and Materials Application, ASM Handbook, ASM International, Materials Park, OH (2007).

[3] F.S. Pettit and G.H. Meier, Oxidation and Hot Corrosion of Superalloys, Superalloys, Transaction of Metallurgical, Society of AIME, Warrendale, NY (1985).
[4] D.E.J. Talbot and J.D.R. Talbot, Corrosion Science and Technology, CRC Press & the Fairmont Press, Inc., USA (1997).
[5] M.P. Boyce, Gas Turbine Engineering Handbook, 2nd ed., Gulf Professional Publishing, USA (2002).
[6] J.R. Davis, Nickel, Cobalt, and Their Alloys, ASM International, Materials Park, OH (2000).
[7] I. Gurrappa and R.A. Sambasiva, Surf. Coat. Technol., 201 (2006) 3016–3029.
[8] E. Lvova and D. Norsworthy, J. Mater. Eng. Perform., 10(3) (2001) 299–312.
[9] T.M. Pollock and S. Tin, J. Propul. Pow., 22(2) (2006) 361–374.
[10] Y. Saito, B. Önay and T. Maruyama, High Temperature Corrosion of Advanced Materials and Protective Coatings, Elsevier Science Publications, North Holland (1992).
[11] M.J. Donachie and S.J. Donachie, Superalloys: A Technical Guide, 2nd ed., ASTM International, Materials Park, OH (2002).
[12] S.D. Cramer and B.S. Covino, Corrosion: Fundamentals, Testing, and Protection, ASM Handbook, Vol. 13A, Materials Park, OH (2003).
[13] S.D. Cramer and B.S. Covino, Corrosion: Materials, ASM Handbook, Vol. 13B, Materials Park, OH (2005).
[14] S.D. Cramer and B.S. Covino, Corrosion: Environments and Industries, ASM Handbook, Vol. 13C, Materials Park, OH (2006).
[15] M. Adam Khan, S. Sundarrajan and S. Natarajan, Surf. Eng., 30(9) (2014) 656–661.
[16] S. Kamal, R. Jayaganthan and S. Prakash, Surf. Eng., 26(7) (2010) 453–462.
[17] R.A. Mahesh, R. Jayaganthan and S. Prakash, Surf. Eng., 26(6) (2010) 413–421.
[18] A. Rahman, R. Jayaganthan, S. Prakash, V. Chawla and R. Chandra, Surf. Eng., 27(5) (2011) 393–401.
[19] S. Kamala, R. Jayaganthan, S. Prakash and S. Kumar, J. Alloy Compd., 463 (2008) 358–372.
[20] E. Liu, Z. Zheng, X. Guan, J. Tong, L. Ning and Y. Yu, J. Mater. Sci. Technol., 26(10) (2010) 895–899.
[21] M. Adam Khan, S. Sundarrajan, S. Natarajan, P. Parameswaran and E. Mohandas, Mater. Manuf. Process, 29 (2014) 1–8.
[22] P.S. Sidky and M.G. Hocking, Corros. Sci., 27(2) (1987) 183–203.
[23] N. Bala, H. Singh and S. Prakash, Mater. Des., 31 (2010) 244–253.
[24] A. Rahman, V. Chawla, R. Jayaganthan, R. Chandra and R. Ambardar, Mater. Chem. Phys., 126 (2011) 253–261.
[25] R.A. Rapp, Corros. Sci., 44 (2002) 209–221.
[26] H.C. Graham and H.H. Davis, J. Am. Ceram. Soc., 54(2) (1971) 89–93.
[27] M.H. Guo, Q.M. Wang, P.L. Ke, J. Gong, C. Sun, R.F. Huang and L.S. Wen, Surf. Coat. Technol., 200 (2006) 3942–3949.
[28] T. Ohji, J. Matyas, N.J. Manjooran, G. Pickrell and A. Jitianu, Advances in Materials Science for Environmental and Energy Technologies III: Ceramic Transactions, Vol. 250, The American Ceramic Society, John Wiley & Sons, USA (2014).
[29] E.J. Opila, High Temperature Corrosion and Materials Chemistry IV: Proceedings of the International Symposium, The Electrochemical Society, USA (2003).
[30] R.A. Rapp and Y.S. Zhang, J. Mater., 46(12) (1994) 47–55.